

RSC Advances



This is an *Accepted Manuscript*, which has been through the Royal Society of Chemistry peer review process and has been accepted for publication.

Accepted Manuscripts are published online shortly after acceptance, before technical editing, formatting and proof reading. Using this free service, authors can make their results available to the community, in citable form, before we publish the edited article. This *Accepted Manuscript* will be replaced by the edited, formatted and paginated article as soon as this is available.

You can find more information about *Accepted Manuscripts* in the [Information for Authors](#).

Please note that technical editing may introduce minor changes to the text and/or graphics, which may alter content. The journal's standard [Terms & Conditions](#) and the [Ethical guidelines](#) still apply. In no event shall the Royal Society of Chemistry be held responsible for any errors or omissions in this *Accepted Manuscript* or any consequences arising from the use of any information it contains.

Length-dependent rectification and negative differential resistance in heterometallic n-alkanedithiol junctions

Jian Shao^{ad}, X. Y. Zhang^{acd}, Yue Zheng^{*abd}, Biao Wang^{*ac} and Yun Chen^{ad}

The transport property of the heterometallic n-alkanedithiol junctions has been investigated via the first-principles calculation. Results show that the heterometallic n-alkanedithiol junctions exhibit significant rectification at lower voltage. The negative differential resistance has also been found at higher voltage, which increases with the increase of n-alkanedithiol backbone length. In order to explain these phenomena, the molecular orbitals of n-alkanedithiol have been analyzed between certain electrodes. It is found that the rectification is induced by asymmetric orbital profiles between the heterometallic electrodes, and negative differential resistance arises when the molecular orbitals cross the band edge provided by metal-sulfur bond.

Introduction

Molecular electronic devices¹ are attracting booming interests for their inherent advantages in both size and bio-affinity over inorganic counterparts². Single-molecule junction^{3, 4} is the most basic component of molecular device. Interesting transport phenomena have been observed in single-molecule junctions, such as rectification^{5,6} and negative differential resistance⁷ (NDR). These effects are fundamental and promising in building single molecular circuits. Rectification in single-molecule junction can be induced by two mechanisms, i.e. the donor- σ -acceptor system and the asymmetric couplings of molecule to the electrodes^{5,8,9}. Previous studies were more focused on the rectification induced by the asymmetry of central molecule^{10,11}. Meanwhile, investigations into the effect of asymmetric electrodes on the molecular rectification have just begun. Typical works like Chen et al.¹² exhibited an obvious rectification in symmetric molecule bridged Au/Pt nanowire heterojunction. Dalglish et al.¹³ investigated the 4-alkanedithiol junctions with heterometallic electrodes via a semi-empirical Extended-Huckel model¹⁴, and found rectification in the junctions due to lack of d-orbital near Fermi level in one of the electrodes. Moreover, some investigations¹⁵ also suggested that molecular junctions with the rectification effect often show combined NDR, which is invoked by resonant tunneling when the molecule is weakly coupled to the electrode¹⁶.

It is well known that the transport properties of single molecular junction¹⁷⁻²⁰ are determined by the level alignment and localization of molecular orbitals²¹. Meanwhile, electrodes play an important role by coupling with the molecular orbital.

Compared with symmetric electrodes, heterometallic electrodes²² induce asymmetric hybridizations in opposite interfaces and can bring additional controllability to molecular junctions. Due to the complexity of the molecule-electrode interaction, the interface should be scrutinized in details. Moreover, the different work functions of the heterometallic electrodes produce a built-in electric field²³. For a molecule of ~nanometers, this electric field is large enough to shift the molecular levels and may bring new characteristics to the junction. So far, it is still unknown how the molecular orbital reacts to the built-in electric field and how much this effect can alter the current²⁴. In addition, because the distribution of electrons in molecule is highly restricted and anisotropic, the localization of orbitals should be strongly dependent on the length of the bridging molecule. Until now, however, how the length of the molecule will affect the transport properties like rectification and NDR in single-molecule junction has not been fully investigated. Thus a comprehensive study is imminent to clarify the problems.

In this paper, the bias dependent transport properties of heterometallic n-alkanedithiol junctions with different backbone lengths have been calculated via the first-principles simulations. A significant rectification of heterometallic n-alkanedithiol junctions has been found. NDR effect has also been observed, and is dependent on the backbone length of the molecule. To explain the rectification and NDR phenomena, discussions on the influences of electrodes on molecular orbitals of the junctions have been devoted, which put an emphasis on the coupling in molecule-electrode interface and the built-in electric field through the scattering

region.

Method

In our simulation, the alkanedithiol molecule was first optimized in gas phase and then connected to the adatoms on seven layers of metal atoms, as shown in Figure 1. All combination of commensurate Au/Ag/Al asymmetric heterometallic electrodes for the junctions have been investigated, respectively. The density-functional^{26,27} calculations were performed within the generalized gradient approximations of Perdew–Burke–Ernzerhof (GGA-PBE)²⁸. Structural relaxations were implemented in the VASP code²⁹. A plane wave basis set with an energy cutoff of 450eV based on projector augmented wave (PAW) method was utilized. Γ -point Brillouin zone integration was used for relaxation until the force on each atom reached the tolerance limit of 0.05eV/Å.

After relaxation, transport calculations were performed within density functional theory (DFT) based non-equilibrium Green function (NEGF) approach²⁵ using Atomistix ToolKit^{30,31}. Here an energy cutoff of 75 Rydberg was used in the framework of linear combination of atomic orbitals (LCAO) basis set. All atoms in the molecule were modeled with double- ζ plus polarization basis sets and the metal atoms were modeled with single- ζ plus polarization basis sets for efficiency. Self-consistency was achieved using a 4×4 k-point sampling in the two-dimensional Brillouin zone. Then the energy resolved transmission spectrums were calculated respectively at different voltages with an 8×8 k-mesh. Local density of states (LDOS)

with a 21×21 k-mesh was averaged in x-y plane to investigate its variation along z axis. In addition, all the energies in the following sections were calculated relative to the Fermi level.

Results and discussion

The transport properties of Au/n-alkanedithiol/Ag junctions

To illustrate the transport properties of Au/n-alkanedithiol/Ag junctions ('Cn', $n=2,4,6,8,10,12$, marking the number of carbon atoms in backbone), the I-V curves have been plotted in Figure 2(a). For $n \geq 4$, the molecular length dependence of the current is verified by fitting to the general expression $I \propto \exp(-\beta n)$. The concatenate fit value of β is 0.93 ± 0.15 per methylene ($0.75 \pm 0.12 \text{ \AA}^{-1}$), similar to previous experimental results ($0.80 \pm 0.08 \text{ \AA}^{-1}$)³². Inside a $\pm 1.0\text{V}$ range, the absolute current is asymmetric. The I-V relationship is in accordance with Simmons model²³ with a voltage-dependent barrier height. At larger positive voltage, significant NDR can be observed, i.e., the current decreases as the voltage increases in $+1.1\text{V}$ to $+2.0\text{V}$ range. Inside -1.1V to -2.0V range, however, the currents appear to be stable. In addition, the conductance of Au/8-alkanedithiol/Ag junction at zero bias (35nS) locates between Au/8-alkanedithiol/Au junction (20nS) and Ag/8-alkanedithiol/Ag junction (50nS). For C2 junction, the current is obviously larger compared with Simmons model over -0.2V to -0.6V range, and thus shows NDR in -0.6V to -1.0V range. This phenomenon is caused by a different transport mechanism, which will be discussed later. For voltages outside a $\pm 1.0\text{V}$ range, the electric field applied on C2 junction was

too strong and destabilized the molecule, so we discarded these data. In summary, all Au/n-alkanedithiol/Ag junctions show asymmetric I-V characteristics under electric field with opposite directions. For comparison, no asymmetric current or NDR has been found in symmetric Au/n-alkanedithiol/Au junction up to $\pm 3\text{V}$ according to Cui et al.³³

The asymmetry of the I-V characteristics has been further illustrated by the rectification ratio I_+/I_- with voltage dependence (see Fig. 2(b)). It is found that the rectification ratio is dependent on both voltages and molecular length. Rectification ratio of C_n junction with $n \geq 4$ increases to as much as 2 at 1V with an identical slope, and it decreases in 1V to 2V range with the effect of NDR. It is also found that the NDR is clearly dependent on molecular length because the rectification ratios reduce more steeply with the increase of molecular length. In contrast, the rectification ratio in C₂ junction is much smaller than the others, indicating a critical length effect. Specifically, the rectification ratio oscillates until the voltage reaches 0.7V and then increases obviously in 0.7V to 1.0V range. The valley near 0.5V is induced by an obscure current increase in -0.2V to -0.7V range. Similar results have also been observed in junctions with Au/Al and Ag/Al electrodes.

The local density of states and molecular projected self-consistent Hamiltonian

In order to explain the rectification in C_n junctions with $n \geq 4$, the molecular projected self-consistent Hamiltonian (MPSH) levels of the heterometallic junctions have been analyzed. It is found that the degenerate molecular energy levels split up to

0.5eV due to heteroelectrodes. This energy level split is introduced by two asymmetry factors: first, the asymmetric hybridization of degenerate molecular orbital with the left and right electrodes; second, the built-in electric field. The first factor of C8 junction has been visualized in LDOS along transport direction, as shown in Figure 3(a). It is found that the extra *5d* orbital in Au compared with Ag leads to asymmetric local density of surface states in -2.5eV to -1.5eV, i.e., high density for Au-S bond (part 3 in Fig. 3(a)) and low density for Ag-S bond (part 4 in Fig. 3(a)). Thus the degenerate orbitals hybrid their energy levels to the asymmetric surface states and split into MPSH eigenstates A and B (shown in red and blue dashed lines in Fig. 4(b)). Meanwhile, the MPSH eigenstates A and B are broaden into density of states (DOS), $D_i(E) = (\gamma_i / 2\pi) / [(E - E_i)^2 + (\gamma_i / 2)^2]$, where $\gamma_i(E) = \gamma_{iL}(E) + \gamma_{iR}(E)$, γ_{iL} and γ_{iR} are the self-energy (or the coupling) of level $i=A$ or B due to left and right electrodes, respectively. As a consequence, the C_{2h} symmetry of the molecule is broken due to the connection with the heterometallic electrodes. On the other hand, the built-in electric field is induced by the difference in the work functions of the two electrodes. In Au/Ag heteroelectrodes, the difference is ~ 1 eV. As illustrated in Figure 4(a), the MPSH eigenstates A and B are separated by the insulating saturate bonds and are localized respectively onto the left and right end of the molecule. So the built-in electric field produces a voltage drop and realigns the energy levels of the two states (shown in red and blue solid lines in Fig. 4(b)). Due to these two factors, the junctions will exhibit rectification under bias. This is because the MPSH levels A and B will further shift $\pm 0.45eV_b$ in opposite directions under applied voltage V_b as

illustrated in Figure 4(c). The energy resolved transmission spectrums are plotted in Figure 4(d). It is shown that the peaks are in correspondence with MPSH eigenstates. According to Landauer-Büttiker (LB) formula³³⁻³⁶, only the transmission within the bias window over $-eV_b/2$ to $eV_b/2$ range, dashed lines in Fig. 4(d)) contributes to current $I = \frac{e}{h} \int_{-eV_b/2}^{eV_b/2} T(E)dE$. It is found that the peak induced by MPSH eigenstate B locates inside the bias window at positive voltages while no peak goes into bias window at negative voltages. As a result, the current under positive voltage is larger than that under negative voltage and the junction rectifies. The rectification can also be fitted to Simmons model²³ if the transmission barrier height is defined as $\Phi_B(V_b) = \Phi_B(0) - 0.45eV_b$. For other asymmetric electrodes like Au/Al, asymmetric movements of energy levels can also be observed (see Table II) and rectification can be expounded in similar ways.

Our second important discovery is the length dependent NDR effect found in +1.1V to +2V range. The arising of NDR at +1V for all heterojunctions in this work is caused by the crossing of MPSH level B through the band edge provided by Au-S bond (see Fig. 3(e)(f)). Interestingly, the peak-valley ratio of NDR increases with the increase of the n-alkanedithiol backbone length (see Fig. 2). This is because the coupling of the molecular orbital with electrode is strongly dependent on its localization. As the molecule becomes longer, the MPSH eigenstate B remains localized on the right end of the molecule and thus its coupling with left electrode is weaker. According to the expression of $D_i(E)$, a smaller coupling leads to a sharper DOS broadening and consequently a steeper NDR effect. On the contrary, no

significant NDR is observed at -1V because MPSH level A locates inside the band provided by Ag-S bond (see Fig. 3(c)(d)).

Length-dependent rectification in heterometallic n-alkanedithiol junctions

Another interesting length-dependent effect is the transition in transport mechanism from C2 to longer junctions. For longer junctions, the transport is dominated by the tunneling through MPSH eigenstates A and B and the contributions from MPSH eigenstates C and D are ignorable. For C2 junction, however, contributions from MPSH eigenstates C' and D' can modify the current significantly. It is found in C2 junction the MPSH eigenstates C' and D' become delocalized through the backbone (see Fig. 5(a)), compared with localized MPSH eigenstates C and D in longer junctions (for example C8 junction in Fig. 4(a)). As shown in Figure 5(b), this delocalization leads to new peaks in energy resolved transmission spectrums. Since the peak invoked by MPSH eigenstates D' locates near the Fermi level, it dominates the current under bias. So C2 junction shows different I-V and rectification characteristics from longer junctions (see Fig. 2(a)(b)).

Conclusions

In summary, we have presented that n-alkanedithiol bridged heterometallic junctions exhibit length-dependent rectification and NDR effects via DFT calculations. The rectification is explained by the molecular level split due to the asymmetric hybridizations with the electrodes and the built-in electric field caused by

difference in electrodes' work functions. The rectification of 2 is by no means large, however one should aware that the junction is bridged by symmetric n-alkanedithiols. Besides, unlike Au/Pt electrodes, the Au/Ag electrodes are in the same group and have similar bonding energies with thiol. Thus the asymmetric properties come mainly from explicit electronic structure at the interface. Significant improvement can be made by combining with appropriate asymmetric molecules or conformations in the interface. In addition, length-dependent NDR in single-molecule junction has been observed. The mechanisms of NDR and length-dependent rules are also investigated to give essential insight and reference for regulating heterometallic n-alkanedithiol junctions. By considering the asymmetric nature, our results could be helpful to reveal the electrodes' availability in manipulating single molecular devices.

Acknowledgements

The authors gratefully acknowledge the financial support of NSFC (Nos. 11402312, 51172291, 11232015, 11474363). Yue Zheng also thanks support by the Fundamental Research Funds for the Central Universities to Micro&Nano Physics and Mechanics Research Laboratory, NCET in University, Research Fund for the Doctoral Program of Higher Education, and Fok Ying Tung Foundation, Science and Technology Innovation Project of Guangdong Provincial Education Department, Guangdong Natural Science Funds for Distinguished Young Scholar and China Scholarship Council.

Notes and references

^aState Key Laboratory of Optoelectronic Materials and Technologies, School of Physics and Engineering, Sun Yat-sen University, 510275, Guangzhou, China; E-mail: zhengy35@mail.sysu.edu.cn; Tel: +86-20-8411-3231

^bDepartments of Mechanical Engineering and Civil and Environmental Engineering, Northwestern University, Evanston, IL 60208, USA; E-mail: yue.zheng@northwestern.edu; Tel: +1-224-999-5961

^cSino-French Institute of Nuclear Engineering and Technology, Sun Yat-Sen University, Guangzhou 510275, China; E-mail: wangbiao@mail.sysu.edu.cn; Tel: +86-20-8411-5692

^dMicro&Nano Physics and Mechanics Research Laboratory, School of Physics and Engineering, Sun Yat-sen University, 510275, Guangzhou, China; E-mail: zhengy35@mail.sysu.edu.cn; Tel: +86-20-8411-3231

- ¹ A. Nitzan and M. A. Ratner, *Science* **300**, 1384 (2003).
- ² H. Hakkinen, *Nat. Chem.* **4**, 443 (2012).
- ³ M. Elbing, R. Ochs, M. Koentopp, M. Fischer, C. von Hanisch, F. Weigend, F. Evers, H. B. Weber, and M. Mayor, *Proc. Natl. Acad. Sci. U. S. A.* **102**, 8815 (2005).
- ⁴ S. Y. Quek, L. Venkataraman, H. J. Choi, S. G. Louie, M. S. Hybertsen, and J. B. Neaton, *Nano Lett.* **7**, 3477 (2007).
- ⁵ A. Aviram and M. A. Ratner, *Chem. Phys. Lett.* **29**, 277 (1974).
- ⁶ N. J. Geddes, J. R. Sambles, D. J. Jarvis, W. G. Parker, and D. J. Sandman, *Appl. Phys. Lett.* **56**, 1916 (1990).
- ⁷ J. Chen, M. A. Reed, A. M. Rawlett, and J. M. Tour, *Science* **286**, 1550 (1999).
- ⁸ J. Taylor, M. Brandbyge, and K. Stokbro, *Phys. Rev. Lett.* **89**, 138301 (2002).
- ⁹ Y. Xue and M. Ratner, *Phys. Rev. B* **68**, 115407 (2003).
- ¹⁰ P. E. Kornilovitch, A. M. Bratkovsky, and R. Stanley Williams, *Phys. Rev. B* **66**, 165436 (2002).
- ¹¹ I. Diez-Perez, J. Hihath, Y. Lee, L. Yu, L. Adamska, M. A. Kozhushner, Oleynik, II, and N. Tao, *Nat. Chem.* **1**, 635 (2009).

- ¹²X. Chen, S. Yeganeh, L. Qin, S. Li, C. Xue, A. B. Braunschweig, G. C. Schatz, M. A. Ratner, and C. A. Mirkin, *Nano Lett.* **9**, 3974 (2009).
- ¹³H. Dalglish and G. Kirzenow, *Phys. Rev. B* **73**, 245431 (2006).
- ¹⁴R. Hoffmann, *J. Chem. Phys.* **39**, 1397 (1963).
- ¹⁵L. Esaki, *Phys. Rev.* **109**, 603 (1958).
- ¹⁶Y. Xue, S. Datta, S. Hong, R. Reifengerger, J. I. Henderson, and C. P. Kubiak, *Phys. Rev. B* **59**, R7852 (1999).
- ¹⁷J. Reichert, R. Ochs, D. Beckmann, H. B. Weber, M. Mayor, and H. von Lohneysen, *Phys. Rev. Lett.* **88**, 4 (2002).
- ¹⁸F. Chen, J. Hihath, Z. F. Huang, X. L. Li, and N. J. Tao, in *Annu. Rev. Phys. Chem.* (Annual Reviews, Palo Alto, 2007), Vol. 58, pp. 535.
- ¹⁹S. M. Lindsay and M. A. Ratner, *Adv. Mater.* **19**, 23 (2007).
- ²⁰S. J. van der Molen and P. Liljeroth, *J. Phys.: Condens. Matter* **22**, 30 (2010).
- ²¹S. Datta, *Quantum transport: atom to transistor*. (Cambridge University Press, 2005).
- ²²J. A. Malen, S. K. Yee, A. Majumdar, and R. A. Segalman, *Chem. Phys. Lett.* **491**, 109 (2010).
- ²³J. G. Simmons, *J. Appl. Phys.* **34**, 1793 (1963).
- ²⁴V. B. Engelkes, J. M. Beebe, and C. D. Frisbie, *J. Am. Chem. Soc.* **126**, 14287 (2004).
- ²⁵Y. Q. Xue, S. Datta, and M. A. Ratner, *Chem. Phys.* **281**, 151 (2002).
- ²⁶P. Hohenberg and W. Kohn, *Phys. Rev.* **136**, B864 (1964).

- ²⁷W. Kohn and L. J. Sham, *Phys. Rev.* **140**, A1133 (1965).
- ²⁸J. P. Perdew, K. Burke, and M. Ernzerhof, *Phys. Rev. Lett.* **78**, 1396 (1997).
- ²⁹G. Kresse and J. Furthmüller, *Phys. Rev. B* **54**, 11169 (1996).
- ³⁰M. Brandbyge, J.-L. Mozos, P. Ordejón, J. Taylor, and K. Stokbro, *Phys. Rev. B* **65**, 165401 (2002).
- ³¹M. S. José, A. Emilio, D. G. Julian, G. Alberto, J. Javier, O. Pablo, and S.-P. Daniel, *J. Phys.: Condens. Matter* **14**, 2745 (2002).
- ³²B. Xu and N. Tao, *Science* **301**, 1221 (2003).
- ³³X. D. Cui, X. Zarate, J. Tomfohr, O. F. Sankey, A. Primak, A. L. Moore, T. A. Moore, D. Gust, G. Harris and S. M. Lindsay, *Nanotechnology* **13**, 5 (2002).
- ³⁴R. Landauer, *IBM Journal of Research and Development* **1**, 223 (1957).
- ³⁵R. Landauer, *Philos. Mag.* **21**, 863 (1970).
- ³⁶M. Büttiker, *Phys. Rev. B* **38**, 9375 (1988).
- ³⁷M. Büttiker, *Ann. N.Y. Acad. Sci.* **581**, 176 (1990).

CHARTS AND FIGURES

Table I. Composition and levels of MPSH eigenstates of C8 between Au/Ag

| Eigenstate | Composition | +1V(eV) | -1V (eV) |
|--------------|---------------------------------------|---------|----------|
| Eigenstate A | Au-S-(CH ₂) ₈ | -2.00 | -1.18 |
| Eigenstate B | (CH ₂) ₈ -S-Ag | -0.60 | -1.52 |
| Eigenstate C | Au-S-CH ₂ | -1.30 | -0.38 |
| Eigenstate D | CH ₂ -S-Ag | -0.09 | -0.85 |

Table II. Composition and levels of MPSH eigenstates of C8 between Au/Al

| Eigenstate | Composition | +1V(eV) | -1V (eV) |
|--------------|---------------------------------------|---------|----------|
| Eigenstate E | Au-S-(CH ₂) ₈ | -2.17 | -1.28 |
| Eigenstate F | (CH ₂) ₈ -S-Al | -1.99 | -2.77 |
| Eigenstate G | Au-S-CH ₂ | -1.33 | -0.41 |
| Eigenstate H | CH ₂ -S-Al | -1.03 | -1.84 |

FIGURE CAPTIONS

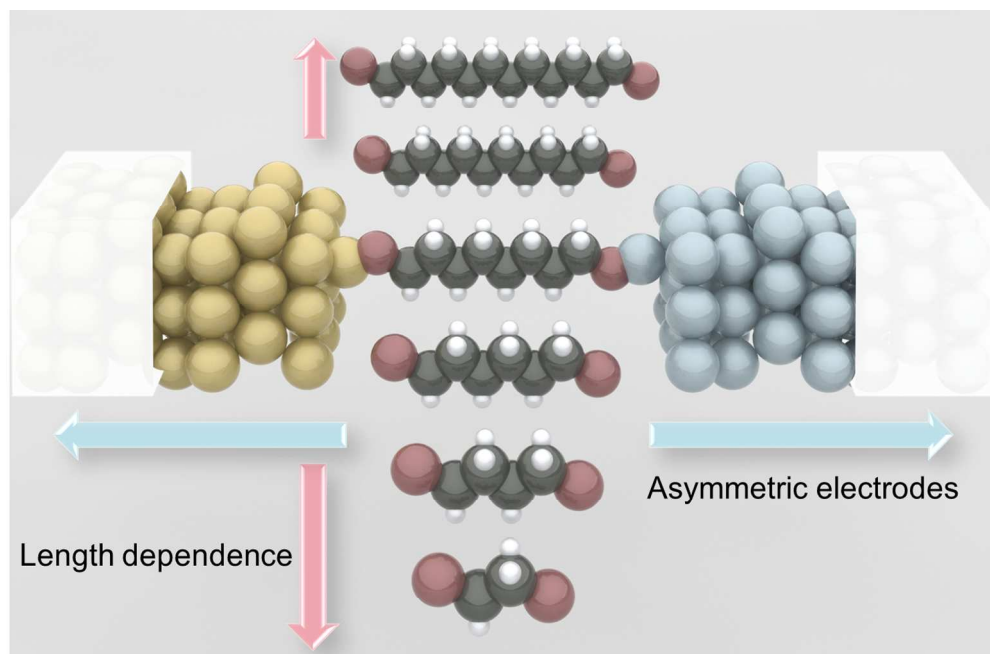
Fig. 1 Schematic illustration of the atomic structure of Au/n-alkanedithiol/Ag heterometallic junctions ($n=2, 4, 6, 8, 10, 12$). Atomic species are shown in colors: yellow for Au, silver for Ag, red for S, black for C, white for H. The whole scattering region is shown and the two glassy boxes indicate the unit cells of the periodic half-infinite structure.

Fig. 2 (a) The absolute currents of C n junctions with $n=2,4,6,8,10,12$ versus voltages (up panel) and fitted slope β in $I \propto \exp(-\beta n)$ for C n junctions with $n=4-12$, together with error bars at each voltage (down panel). (b) The I_+/I_- versus absolute voltage of C n junctions with $n=2-12$.

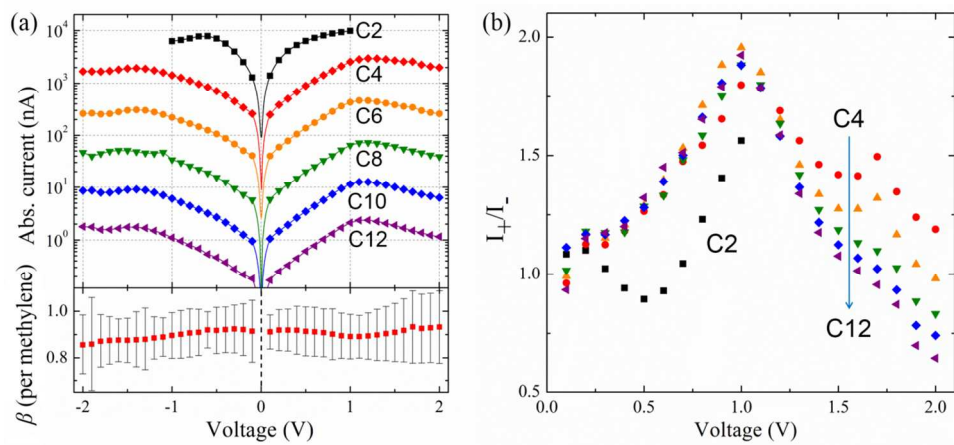
Fig. 3 (a) LDOS at equilibrium averaged in x - y plane and the atomic structure of C8 junction in real space with the same z axis. The white area shows LDOS beyond the upper limit of the color bar (very high DOS). The dashed line indicates the average Fermi level. LDOS in part 5 is plotted aside in (b) with a fiftieth contour value of (a). For $-1V$ and $+1V$, the LDOS in scattering region and part 5 are shown in (c)-(f) respectively.

Fig. 4 (a) MPSH eigenstates (0.02 absolute contour cleave) of C8 junction marked as A, B, C and D. (b) Schematic illustrations of molecular level movement during bridging between heterometallic electrodes at equilibrium. The black solid line indicates the potential energy drop caused by the built-in electric field. (c) The energy level movements of MPSH eigenstates A (red) and B (blue) from $-1V$ to $+1V$. (d) The energy resolved transmission spectrums of C8 junction under bias.

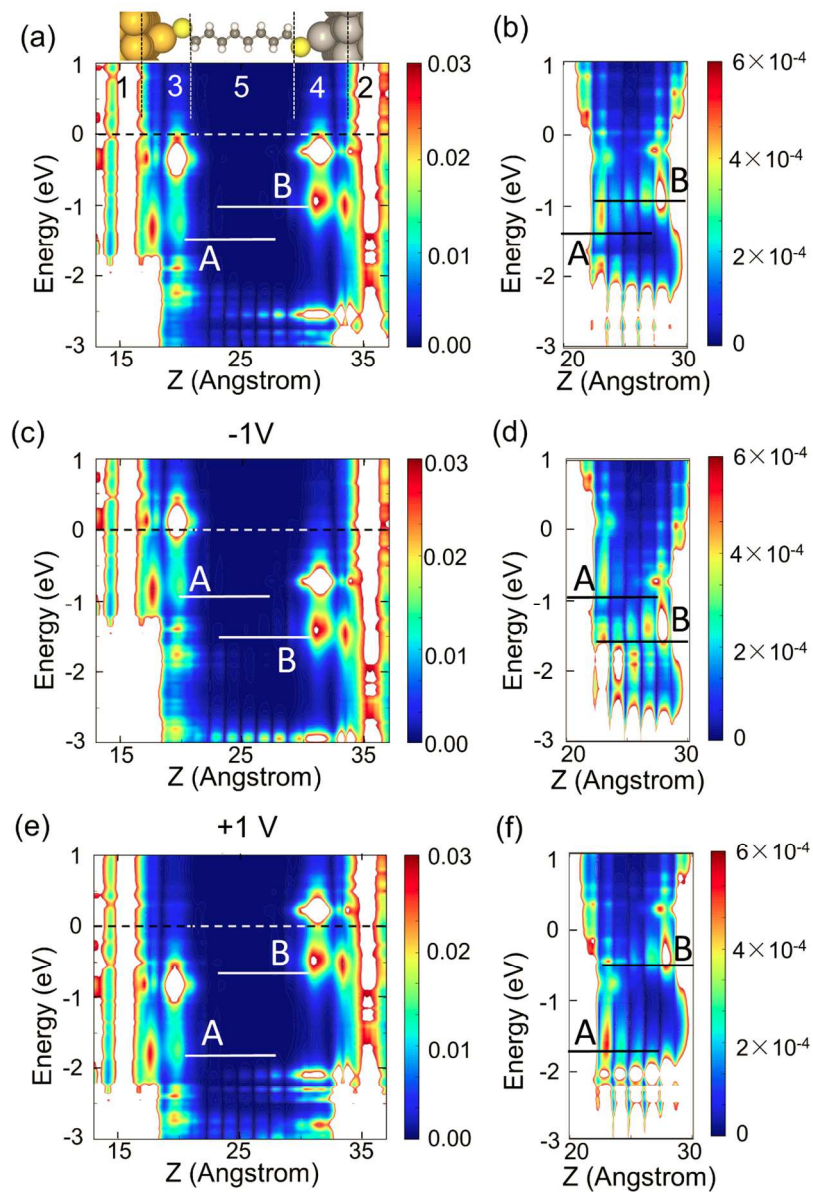
Fig. 5 (a) MPSH eigenstates (0.02 absolute contour cleave) of C2 junction marked as A', B', C' and D'. (b) The energy resolved transmission spectrums at equilibrium of C n junctions ($n=2,4,6,8$).



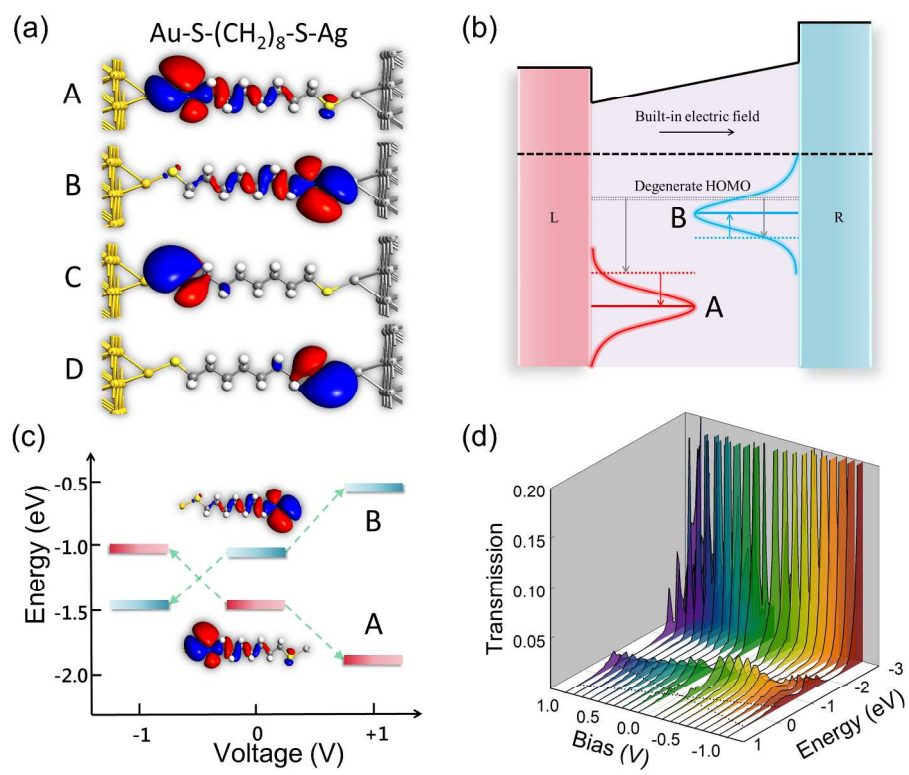
395x270mm (96 x 96 DPI)



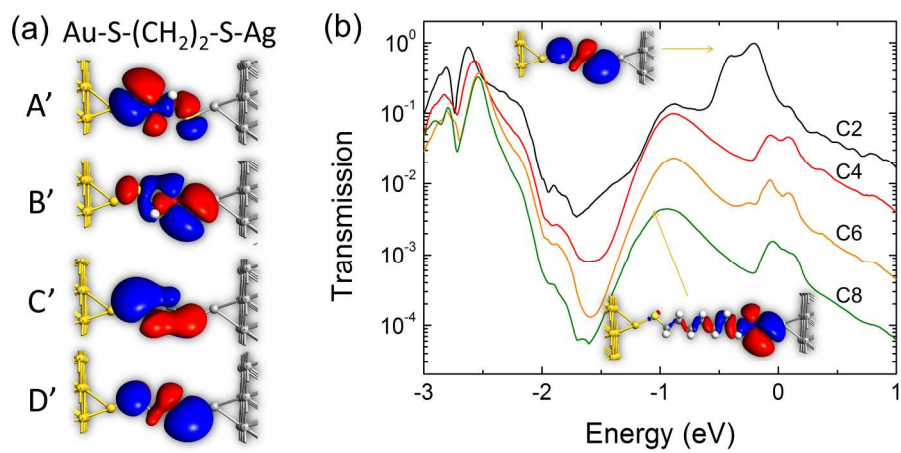
375x171mm (96 x 96 DPI)



323x476mm (96 x 96 DPI)



670x526mm (96 x 96 DPI)



623x309mm (96 x 96 DPI)